Imaging Phase Separation near the Mott Boundary of the Correlated Organic Superconductors κ-(BEDT-TTF)2X

doi: 10.1103/PhysRevLett.92.227001

Imaging Phase Separation near the Mott Boundary of the Correlated Organic Superconductors κ-(BEDT-TTF)$_2X$

T. Sasaki,[1] N. Yoneyama,[1] N. Kobayashi,[1] Y. Ikemoto,[2] and H. Kimura[2]

[1]*Institute for Materials Research, Tohoku University, Katahira 2-1-1, Sendai 980-8577, Japan*

[2]*SPring-8, Japan Science Radiation Research Institute, Mikazuki, Hyogo 679-5198, Japan*

(Received 4 February 2004; published 2 June 2004)

Electronic phase separation consisting of the metallic and insulating domains with 50–100 μm in diameter is found in the organic Mott system κ-[(h8-BEDT-TTF)$_{1-x}$(d8-BEDT-TTF)$_x$]$_2$Cu[N(CN)$_2$]Br by means of scanning microregion infrared spectroscopy using the synchrotron radiation. The phase separation appears below the critical end temperature 35–40 K of the first-order Mott transition. The observation of the macroscopic size of the domains indicates a different class of the intrinsic electronic inhomogeneity from the nanoscale one reported in the inorganic Mott systems such as high-T_c copper and manganese oxides.

DOI: 10.1103/PhysRevLett.92.227001 PACS numbers: 74.70.Kn, 71.30.+h, 78.30.Jw

Microscopic spatially inhomogeneous electronic states have been recently observed in many kinds of correlated electron systems. Nanoscale spatial variation of the superconducting gap has been revealed in the superconducting state of $Bi_2Sr_2CaCu_2O_{8+\delta}$ by the scanning tunneling spectroscopy and microscopy [1]. In the normal state, charge carriers doped into antiferromagnetic insulators tend to group into some regions of the sample in the form of stripes in some copper oxides [2]. Meanwhile, a different kind of the microscopic phase separation takes place in half-doped manganese oxides [3]. Small variation from half doping causes phase segregation of electron-rich ferromagnetic and electron-poor antiferromagnetic domains with submicron size within the charge ordered phase. In the system with Mott transition, the nanoscale electronic inhomogeneity with preferred orientation has been found in slightly doped Mott insulator $Ca_{2-x}Na_xCuO_2Cl_2$ [4]. $NiS_{2-x}Se_x$ pyrite, which is the bandwidth controlled Mott system, has shown also microscopic electronic inhomogeneity at the critical vicinity of the metal-insulator transition [5]. These microscopic spatial electronic inhomogeneities seem to be of intrinsic nature near the criticality of changes in charge, spin, orbital, and lattice degrees of freedom in the correlated electron system.

Organic charge transfer salts based on the donor molecule bis(ethylenedithio)-tetrathiafulvalene, abbreviated BEDT-TTF or ET, have been recognized as one of the highly correlated electron systems [6]. Among them, κ-(ET)$_2X$ with $X = Cu(NCS)_2$, Cu[N(CN)$_2$]Y (Y = Br and Cl), etc. have attracted considerable attention from the point of view of the strongly correlated quasi-two-dimensional electron system because the strong dimer structure consisting of two ET molecules makes the conduction band effectively half filling [7–9]. The unconventional metallic, antiferromagnetic insulating, and superconducting phases appear next to one another in the phase diagram [7,10,11]. The transitions among these phases are controlled by the applied pressure [11] and slight chemical substitution of the donor and anion molecules [12], which must change the conduction band width W with respect to the effective Coulomb repulsion U between two electrons on a dimer. Thus, the κ-(ET)$_2X$ family has been considered to be the bandwidth controlled Mott system in comparison with the filling controlled one in the inorganic perovskites such as high-T_c copper oxides.

Recently, inhomogeneous electronic states have been suggested in the ^{13}C-NMR experiments near the first-order metal-insulator transition in the artificially bandwidth controlled κ-(ET)$_2$Cu[N(CN)$_2$]Br [13]. Below characteristic temperature T^* where the incoherent bad metallic state changes to the coherent good metal at lower temperature [14], ^{13}C-NMR lines fall into two groups indicating the metallic and antiferromagnetic insulating nature. The results imply that two phases coexist spatially and statically. Subsequent transport experiments have also suggested such coexistence of two phases at low temperature [15]. Although it has been demonstrated that an inhomogeneous electronic state is realized near the first-order transition, the detail of the morphology, spatial distribution, size of domains, and stability of the inhomogeneity have not been clarified yet. It is very important to obtain the real space information which can give us a clue to know either similar nanoscale electronic inhomogeneity is realized by the exotic mechanism based on the strong correlation effect or macroscopic phase separation occurs due to local potential modulation near the first-order transition.

In this Letter, we present the real space imaging of the electronic phase separation in the partly substituted κ-[(h8-ET)$_{1-x}$(d8-ET)$_x$]$_2$Cu[N(CN)$_2$]Br, where h8-ET and d8-ET denote fully hydrogenated and deuterated ET molecules, respectively. Scanning microregion infrared reflectance spectroscopy (SMIS) using the synchrotron radiation (SR) is applied to make the two-dimensional

map of the local electronic state. The results indicate that the macroscopic electronic phase separation takes place near the first-order metal-insulator transition, which is different from the nanoscale electronic inhomogeneity in the inorganic correlated electron system.

Single crystals of κ-$[(h8\text{-ET})_{1-x}(d8\text{-ET})_x]_2$-$Cu[N(CN)_2]Br$ partly substituted by deuterated ET molecule were grown by the standard electrochemical oxidation method. The substitution x denotes the nominal mole ratio to the fully deuterated ET molecule in the crystallization. We checked the actual substitution with respect to the nominal value x by measuring the intensity of the molecular vibrational mode of the terminal ethylene groups. The substitution dependence of the macroscopic phase diagram and the superconducting properties have been examined [16]. The full volume of the superconductivity has been observed in the range $x = 0$–0.5 when the samples are cooled slowly. Above $x = 0.5$, however, the superconducting volume fraction decreases and becomes about a few tens of vol % at $x = 1$, a value which strongly depends on the cooling condition.

SMIS measurements were performed using SR at BL43IR in SPring-8 [17]. The polarized reflectance spectra were measured on the c-a plane along the $E \parallel a$ axis and the $E \parallel c$ axis with a Fourier transform spectrometer and a polarizer in the midinfrared (IR) range. An IR microscope with the controlled precision x-y stage and high intensity of SR light enables us to obtain the two-dimensional reflectance spectrum map with the spatial resolution of ~ 10 μm [18]. The sample was fixed by the conductive carbon paste on the sample holder with a gold mirror which was placed at the cold head of the helium flow-type refrigerator. The reflectivity was obtained by comparison with the gold mirror at each temperature measured.

In order to make the real space image of the electronic states on the crystal surface by SMIS measurements, we use the shift of the frequency ω_3 of a molecular vibration mode $\nu_3(a_g)$. The specific $\nu_3(a_g)$ mode, which is a symmetric stretching mode of the central double bonded carbon atoms of the ET molecule, has been found to be very sensitive to the difference between metallic and insulating states due to the large electron-molecular vibration coupling [14]. The peak of the $\nu_3(a_g)$ mode should shift to a lower frequency in a sharper shape in the insulating state at low temperature, while it shows the opposite feature in the metallic state. Figure 1 shows the two-dimensional contour map of the reflectivity peak frequency ω_3 of $\nu_3(a_g)$ at 4 K in κ-$[(h8\text{-ET})_{1-x}(d8\text{-ET})_x]_2Cu[N(CN)_2]Br$ of (a) $x = 0.5$ and (b) $x = 0.8$. The polarized reflectance spectra ($E \parallel c$ axis and $E \parallel a$ axis) in the microregion of ~ 10 μm ϕ are taken with a step of 15 and 10 μm for $x = 0.5$ and 0.8 samples, respectively. The typical reflectivity spectra of $\nu_3(a_g)$ in the $E \parallel c$ axis are shown in Fig. 2(c), taken at the O point in the dark color region and the B' point in the

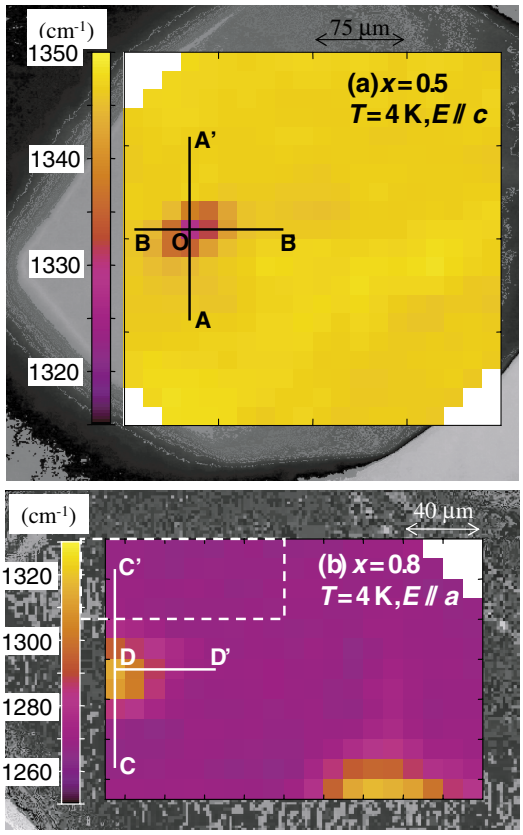

FIG. 1 (color online). Two-dimensional contour map of the peak frequency of the $\nu_3(a_g)$ mode on the crystal surface of κ-$[(h8\text{-ET})_{1-x}(d8\text{-ET})_x]_2Cu[N(CN)_2]Br$ with (a) $x = 0.5$ ($E \parallel c$) and (b) $x = 0.8$ ($E \parallel a$) at 4 K. Bright color indicates the metallic nature and dark color does the insulating one. The lines AOA', BOB', CDC', and DD' indicate the scanning lines shown in Figs. 2(a) and 2(b). In the region framed by dashed lines, more fine mapping was performed.

bright color region of the $x = 0.5$ sample. The bright region indicates the higher frequency of ω_3 which demonstrates the metallic feature [19]. It is noted that the different absolute values of ω_3 observed in the metallic (or insulating) region of $x = 0.5$ and 0.8 samples are caused by the polarization dependence of the $\nu_3(a_g)$ mode [14]. Some domains with lower and higher ω_3 can be found in the major metallic and insulating regions in $x = 0.5$ and 0.8, respectively. In $x = 0.5$, the bright region is dominant almost all over the surface. In contrast, the dark region is dominant in $x = 0.8$. The structure and position of the domain are found to be stable on time. The domains seem not to be located at a particular position such as the sample edge, step and scratch of the surface, and so on. The shape is almost circular, and no specific orientation with respect to the crystal axes is observed.

Figures 2(a) and 2(b) show the scanning position dependence of ω_3 around the insulating and metallic domains of $x = 0.5$ and 0.8 samples, respectively. Each domain has a size of around $\sim 50 \times 50$ μm^2. The total insulating area is very roughly estimated to be $\sim 1/40$ and

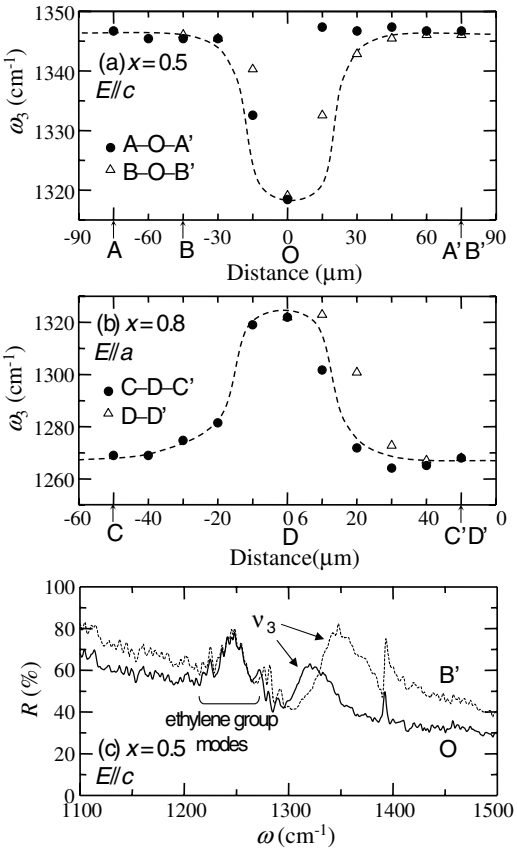

FIG. 2. Space variation of the peak frequency ω_3 of the $\nu_3(a_g)$ mode in κ-$[(h8\text{-ET})_{1-x}(d8\text{-ET})_x]_2\text{Cu}[\text{N}(\text{CN})_2]\text{Br}$ with (a) $x = 0.5$ and (b) $x = 0.8$. The dashed curves are guides for the eyes. The locations O, A, B, ... correspond to the points indicated in Fig. 1. (c) The reflectivity spectra at O and B' points.

$\sim 9/10$ of the measured area for $x = 0.5$ and 0.8 samples, respectively. This insulating fraction reflects the bulk properties obtained by the magnetization measurements [16]. The superconducting volume fraction is almost the same with the sample volume from $x = 0$ to ~ 0.5 in the slow cooling condition. The fraction starts to decrease with increasing x from ~ 0.5 to a higher value. The superconducting volume fraction around $x = 0.75$–0.8 is expected to be in the range of a few tens of vol % in slow cooling and a few vol % in fast cooling. Considering the variation of the fraction with the cooling condition and difference of the evaluation methods, consistency between the bulk magnetization and the present measurements on the metal-insulator fraction is reasonably well.

We have not detected the smaller domain in the present SMIS measurements. Inside the rectangular region framed by dashed lines in Fig. 1(b), more fine mapping (3 μm step) was performed but the spectra were the same with each other. This does not exclude the possibility of the nanoscale inhomogeneity inside each scanning spot because the obtained spectrum may result in the average of nanoscale inhomogeneity in the measured spot. Close agreement between the magnetization and present results suggests that the phase separation occurs on the macroscopic scale.

Possible chemical inhomogeneity to the origin of the domain structure such as segregation of deuterated ET can be excluded by checking the molecular vibration mode of terminal ethylenes of ET at each scanning point. The vibration modes of the ethylene groups and the deuterated one appear at different frequencies around 1250 and 1050 cm^{-1}, respectively. As can be seen in Fig. 2(c), almost the same structure and intensity of the ethylene mode are observed at both O and B' points, which demonstrates the same substitution ratio of the deuterated ET molecule at the insulating and metallic regions. Therefore, the present finding of the domain structure strongly indicates that the electronic phase separation appears in the macroscopic size due to the strong correlation effect near the Mott metal-insulator transition.

In order to know the correlation between the formation of the phase separation and the electronic phase diagram, the temperature variation of the phase separation was measured. Figure 3 shows the two-dimensional contour maps on the reflectivity peak frequency ω_3 of the $\nu_3(a_g)$ mode in the $E \parallel c$ axis at 18, 32, and 46 K in the $x = 0.5$ sample [20]. The scanning region is almost the same with the map at 4 K in Fig. 2(a). The measurements were performed from low (4 K) to high (46 K) temperature in sequence. The insulating domain does not change the position and size at higher temperatures of 18 and 32 K. The domain looks likely to disappear at 46 K. This temperature corresponds to the critical end point $T_{\text{cr}} \simeq 40$ K of the Mott first-order metal-insulator transition [10,11,14]. From T_{cr} to both weak and strong correlation sides in the phase diagram, the T^* line and the bad metal-insulator line T_{ins} are elongated. In temperatures above T_{cr}, T^*, and T_{ins}, the half-filling bad metallic state exists in a wide range of the correlation strength which can be tuned by pressure and substitution of anion. The critical point in the present system has been considered to be located around $x = 0.5$, where the phase separation may start to appear in a larger x value than 0.5 [16]. In the weak correlation side from T_{cr}, which corresponds to the present system with $x \leq \sim 0.5$, the bad metal changes to a correlated good metal through T^* and then becomes superconducting [11,14]. In the strong correlation side, the bad metal develops into a Mott insulator through T_{ins} and then becomes an antiferromagnetic Mott insulator at T_{N} [11,14]. Disappearance of the domain structure at 46 K can be explained by no multielectronic states competing with each other above T_{cr}, T^*, and T_{ins}. On one hand, below T_{cr} the phase separation occurs near the boundary of the first-order transition between the Mott insulator and the correlated good metal.

In the phase separation, the multiple potential minima of the free energy is required in general, and the domain

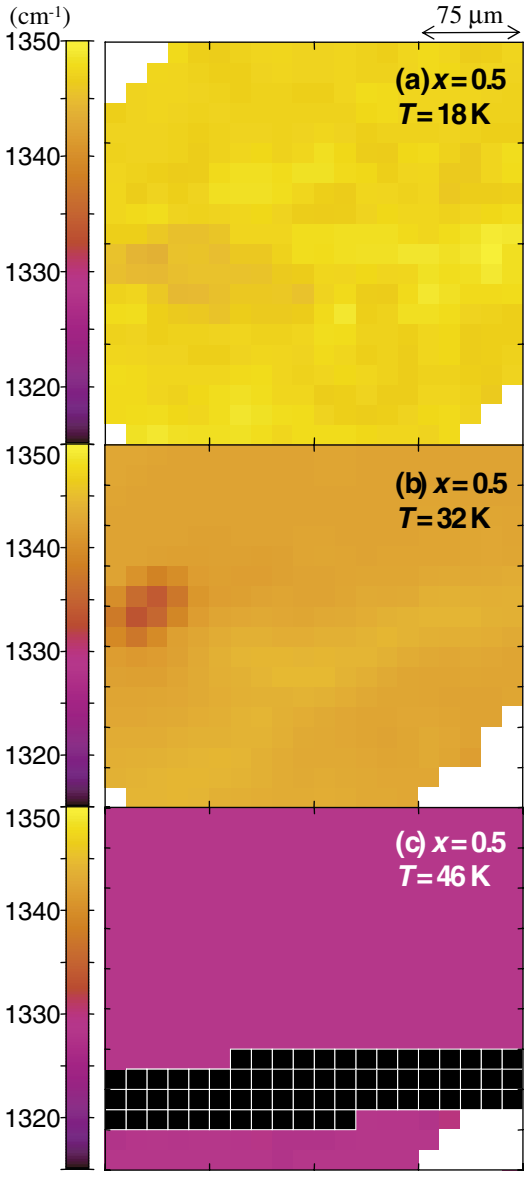

FIG. 3 (color online). Temperature variation of the two-dimensional contour map of the peak frequency of the $\nu_3(a_g)$ mode in the $E \parallel c$ axis in the $x = 0.5$ sample. Imaging region is the same with that in Fig. 1(a). Picture elements are accidentally missing in the lower part of the map at 46 K [20].

grows from a nucleation point which should be specific in the free energy variation in space. The possible origin of the space variation in the free energy is a glassy conformational order-disorder of the terminal ethylene groups of ET molecules [6,21]. The ethylene groups have been known to have the conformational disorder which is frozen by cooling through a temperature $T_{\mathrm{glass}} \simeq 80$ K. The degree of disorder depends on the cooling rate; cooling faster introduces a larger number of disorders. Such disorder has been considered to modulate the electronic states locally [22,23]. The slight modulation of a potential energy in space may become a nucleation point of the domain growth in the phase separation. Indeed the ratio and distribution of the metal-insulator phase separation have appeared to change with different thermal cycles and cooling speed passing through T_{glass}. The detail will be presented elsewhere [24]. In order to make clear the mechanism of the phase separation and the process of the domain formation, a space imaging technique with molecular resolution must be developed.

We are grateful to T. Hirono and T. Kawase for their technical support. SR experiments were performed at SPring-8 with the approval of JASRI (2003A0075-NS1-np and 2003B0114-NSb-np). This work was partly supported by a Grant-in-Aid for Scientific Research (C) (Grant No. 15540329) from JSPS.

[1] K. M. Lang *et al.*, Nature (London) **415**, 412 (2002).
[2] J. M. Tranquada *et al.*, Nature (London) **375**, 561 (1995).
[3] M. Fäth *et al.*, Science **285**, 1540 (1999).
[4] Y. Kohsaka *et al.*, J. Low Temp. Phys. **131**, 299 (2003).
[5] T. Hanaguri *et al.*, Physica C (Amsterdam) (to be published).
[6] M. Lang and J. Müller, in *The Physics of Superconductors*, edited by K. H. Bennenmann and J. B. Ketterson (Springer-Verlag, Berlin, 2003), Vol. II.
[7] K. Kanoda, Hyperfine Interact. **104**, 235 (1997).
[8] H. Kino and H. Fukuyama, J. Phys. Soc. Jpn. **65**, 2158 (1996).
[9] R. McKenzie, Science **278**, 820 (1997).
[10] T. Sasaki *et al.*, Phys. Rev. B **65**, 060505 (2002).
[11] P. Limelette *et al.*, Phys. Rev. Lett. **91**, 016401 (2003).
[12] A. Kawamoto, H. Taniguchi, and K. Kanoda, J. Am. Chem. Soc. **120**, 10 984 (1998).
[13] K. Miyagawa, A. Kawamoto, and K. Kanoda, Phys. Rev. Lett. **89**, 017003 (2002).
[14] T. Sasaki *et al.*, Phys. Rev. B **69**, 064508 (2004).
[15] H. Taniguchi, K. Kanoda, and A. Kawamoto, Phys. Rev. B **67**, 014510 (2003).
[16] N. Yoneyama *et al.*, cond-mat/0402115 [J. Phys. Soc. Jpn. (to be published)].
[17] H. Kimura *et al.*, Nucl. Instrum. Methods Phys. Res., Sect. A **467–468**, 441 (2001).
[18] S. Kimura *et al.*, Nucl. Instrum. Methods Phys. Res., Sect. A **467–468**, 893 (2001).
[19] The metallic region should show superconductivity at 4 K, which is suggested by the bulk magnetization measurements [16]. We cite, however, a metal instead of a superconductivity in the higher frequency region at 4 K because it is difficult to distinguish between two states in the present experimental method.
[20] No picture elements are caused by an accidental interrupt of SR beam.
[21] J. Müller *et al.*, Phys. Rev. B **65**, 144521 (2002).
[22] N. Yoneyama *et al.*, J. Phys. Soc. Jpn. **73**, 184 (2004).
[23] N. Yoneyama *et al.*, J. Phys. Soc. Jpn. **73**, 1290 (2004).
[24] T. Sasaki *et al.* (unpublished).